Case Studies in Construction Materials 16 (2022) e00824

Contents lists available at ScienceDirect

Case Studies in Construction Materials

journal homepage: www.elsevier.com/locate/cscm

Case study

CFRP lamella stay-cable and its force measurement based on microwave radar

Yue Liu [a], Jia-Zhan Xie [a], T. Tafsirojjaman [b], Qing-Rui Yue [c,*], Cheng Tan [d], Gong-Jian Che [e]

[a] The Key Laboratory of Urban Security and Disaster Engineering of Ministry of Education, Beijing University of Technology, 100 Pingleyuan, Beijing, China
[b] Centre for Future Materials (CFM), School of Civil Engineering and Surveying, University of Southern Queensland (USQ), Toowoomba, QLD 4350, Australia
[c] Research Institute of Urbanization and Urban Safety, School of Civil and Resource Engineering, University of Science and Technology Beijing, 30 Xueyuan Road, Beijing, China
[d] College of Civil Engineering, Tongji University, 1239 Siping Road, Shanghai, China
[e] Intelligent Internet of China Communication Co., Ltd., 67 Chaoyang Road, Beijing, China

ARTICLE INFO

Keywords:
CFRP lamella stay-cable
Cable force
Wedge-shaped clamp anchorage
Microwave radar
Vibration frequency method

ABSTRACT

Carbon Fiber Reinforced Polymer (CFRP) has advantageous characteristics such as lightweight, high strength, high corrosion and fatigue resistance, low creep, and high damping, etc. It is suitable to be used in bridge structures as cables, which can effectively solve the problems of easy rusting, heavyweight, low tensile strength, and low fatigue performance of steel cables. This paper firstly illustrates the advantageous properties of CFRP lamella compared with CFRP rod in terms of cable anchoring and then investigates the performance of wedge-shaped clamp anchorage for CFRP lamella cable by finite element analysis and static tensile test. Finally, the process of measuring the cable force of CFRP lamella stay-cable with non-contact microwave cable force measurement technology is introduced. The finite element analysis and experiment show that the wedge-shaped clamp anchorage can effectively anchor the CFRP lamella stay-cable with a relatively high anchorage efficiency, and the maximum stress of the CFRP lamella stay-cable is at the free section instead of the anchorage section, and the failure pattern is mainly the fiber explosion of the free section. The results of microwave cable force measurement are consistent with those of the traditional pressure sensor and strain gauge methods. The non-contact microwave cable force measurement technology is easy and fast to operate, and it is suitable for measuring the force of CFRP cable.

1. Introduction

Carbon Fiber Reinforced Polymer (CFRP) is an advanced composite material with many advantages, such as lightweight, high strength, high corrosion and fatigue resistance, and low relaxation, which makes it suitable to be made into cables [1]. Those advantageous characteristics of CFRP attract scholars to consider replacing steel cables with CFRP ones in engineering structures since

* Corresponding author.
E-mail addresses: yliu@bjut.edu.cn (Y. Liu), xiejiazhan2021@163.com (J.-Z. Xie), tafsirojjaman@usq.edu.au (T. Tafsirojjaman), yueqr@vip.163.com (Q.-R. Yue), tctj21@126.com (C. Tan), 593274961@qq.com (G.-J. Che).

https://doi.org/10.1016/j.cscm.2021.e00824
Received 22 September 2021; Received in revised form 15 November 2021; Accepted 25 November 2021
Available online 26 November 2021
2214-5095/© 2021 The Authors. Published by Elsevier Ltd. This is an open access article under the CC BY-NC-ND license (http://creativecommons.org/licenses/by-nc-nd/4.0/).

the early 1980 s. In 1987, Meier proposed the great vision of building a CFRP cable-stayed bridge with a main span of 8400 m across the Strait of Gibraltar [2]. The first practical application of CFRP cables was used as stay-cables in the Tsukuba FRP footbridge in Japan in 1996 [3]. The 24 stay-cables of the bridge included bond anchored CFRP rod and strand cables. In October of the same year, the research group of Swiss Federal Materials Laboratory replaced two steel stay-cables with CFRP cables in the Stork Bridge in Winterthur, Switzerland, which is the world's first highway cable-stayed bridge using CFRP cables [4]. At present, CFRP cables have already been applied to seven cable-stayed bridges, two prestressed girder bridges, two stress-ribbon bridges, and two suspension bridges [1]. Most of them adopt CFRP rod type cables, whereas CFRP lamellas are usually used in structural reinforcement [5,6].

In order to make full use of CFRP cable's advantages, an anchorage system with sufficient bearing capacity is necessary. Up to now, many anchorage systems for CFRP rod or lamella type cables have been proposed. According to the anchoring mechanism, they can be mainly divided into two types, i.e. bond anchorage and clamp anchorage. Bond anchorage relies on the bond force generated by the bonding medium to anchor the CFRP cable [7]. Meier et al. [8] proposed a bond anchorage for CFRP rod type cables using a conical steel socket and a special binder, which is made of epoxy resin mixed with Al_2O_3 ceramic granules. The density of Al_2O_3 ceramic granules in the epoxy resin increases from the anchorage front to the end forming a gradient stiffness, which can reduce the CFRP stress peak in the anchorage and increase the anchorage efficiency. This anchorage was successfully used to anchor two CFRP parallel rod cables in Stork Bridge, Switzerland. Fang et al. [9] developed a bond anchorage system using ultra-high performance reactive powder concrete (RPC) grout as the bonding medium to anchor CFRP parallel rod tendons, which was successfully applied to Aizhai Bridge, China [10]. Wang et al. [11] designed an integral variable stiffness bond anchorage for large-tonnage FRP rod type cables, in which the bonding medium was composed of four kinds of binders with different stiffness. Static and fatigue tests proved the reliability and validity of this anchorage [12]. Clamp anchorage relies on the clamp function, i.e. the friction force, to anchor the CFRP cable [7]. The clamp anchorage can be further divided into two types, i.e. the wedge type and plate type. For the wedge type clamp anchorage, the clamping force is generated by the extrusion of the CFRP cable; while for the plate type clamp anchorage, the clamping force comes from the fastening of bolts. A wedge type clamp anchorage system was developed by Freyssinet Corp., which uses aluminum sleeves to protect the CFRP rod from local crushing by the steel wedge [13]. CFRP parallel rod cables with these anchorages were used in practice for Laroin Footbridge, France [14]. Andrä and Maier [15] proposed a clamp anchorage for CFRP lamella. It has two clamping plates with a gradually increased cross-sectional area, which makes the anchoring stiffness increase from the anchorage front to the end and hence increasing the anchorage efficiency. Sika Group developed a wedge type clamp anchorage called SIKA Stress Head 220, which uses FRP wedges instead of steel ones to anchor CFRP lamella, so as to avoid the premature failure of CFRP [16]. Furthermore, some researchers also proposed combining the bond and clamp functions together to achieve a better anchoring effect. Li et al. [17] proposed an innovative compound-type anchorage system for FRP rod type cables, which combines mechanical extrusion and chemical bonding to provide reliable anchorage bearing capacity for FRP rods. The finite element analysis, static and fatigue experiments indicated that the stress distribution of the compound-type anchorage was uniform and the anchorage efficiency was satisfactory. In summary, there is no mature solution yet for the anchorage of CFRP cable. The existing CFRP cable anchorages still have various problems, such as complex structure, relatively low efficiency, and high cost, which require further study.

The technology to measure cable force has always been given great importance by engineers in the field of cable supported bridges. The accuracy of cable force measurement directly affects the success of construction, control, inspection and maintenance of cable-stayed bridges. Presently, there are five methods usually used to measure the force of stay-cables, i.e. pressure sensor method, tension jack method, magnetic flux method, strain gauge method and frequency method [18]. The first two methods are convenient to measure the change of the cable force during the tensioning process, but are not convenient for the measurement of the cable force after the completion of the bridge. The magnetic flux and strain gauge methods are costly and inconvenient [19]. At present, the fifth one, i.e. vibration frequency method, is more commonly used. It firstly obtains the natural frequency of the cable and then uses the relationship between the frequency and cable force to calculate the force. The vibration frequency is usually measured by tying the sensor to the cable [20]. However, some non-contact technologies, such as computer vision-based technology [21] and radar interferometry technology [22], have started to be used in this field.

In this paper, a non-contact cable force rapid measurement technology based on microwave radar is used in the cable force measurement test of the CFRP lamella stay-cable. Firstly, the advantages of CFRP lamella cable in terms of anchorage are illustrated by comparing with the CFRP rod. Then, the anchorage performance of a wedge-shaped clamp anchorage for CFRP lamella is investigated by finite element analysis and static tensile test. Finally, the case study of measuring the force of CFRP lamella stay-cable with non-contact microwave radar in a model cable-stayed bridge is introduced. The effectiveness of the CFRP cable force measurement based on microwave radar is confirmed by comparing with those of the pressure sensor and strain gauge methods.

Table 1
Comparison of anchorage area between CFRP rod and lamella.

Type	Geometry (mm)	Cross-sectional area (mm^2)	Anchorage length (mm)	Perimeter of the cross-section (mm)	Anchorage area (mm^2)
CFRP rod-1	8.8(Φ)	60	100	27.6	2760
CFRP rod-2	13.8(Φ)	150	100	43.4	4340
CFRP lamella-1	20(w)× 3(t)	60	100	46	4600
CFRP lamella-2	50(w)× 3(t)	150	100	106	10600

(φ represents the diameter of the CFRP rod, w and t represent the width and thickness of the CFRP lamella respectively).

2. CFRP lamella cable

2.1. Properties of CFRP lamella cable

CFRP rod and lamella are mainly two types of raw materials for CFRP cables. In terms of cables anchorage area, CFRP lamella has a much larger anchorage area than that of CFRP rod under the same conditions. For the same cross-sectional area and anchorage length of the CFRP rod and CFRP lamella, the CFRP lamella has a higher perimeter and higher anchorage area as well, which can be evident from Table 1.

As can be seen, for the CFRP lamella and CFRP rod having consistent cross-sectional area and anchorage length, the anchorage area of the CFRP lamella is approximately twice that of the CFRP rod. Moreover, the anchorage area of CFRP lamella is almost proportionally increasing with the increase of the width (w) of CFRP lamella, which indicates that the CFRP lamella with a wider width has a greater anchorage area compared to the lamella with a narrower width when the thickness is the same. This analysis shows that the CFRP lamella is more efficient to anchor than the CFRP rod as the bond force, friction force and the anchorage bearing capacity increase with the increasing of the anchorage area of CFRP. Admittedly, the above analysis has only considered the anchorage area. Further study is needed to investigate other points of anchorage mechanisms, such as effective anchorage length, stress transfer mechanism, etc.

2.2. Wedge anchorage for CFRP lamella stay-cable

2.2.1. Anchorage design

A wedge-shaped clamp anchorage was developed to anchor the CFRP lamella cable in this work, which is composed of a round anchor barrel and two half-round wedge plates. The schematic and dimensional views of the anchorage structure are shown in Figs. 1 and 2, respectively. The clamping plane between the two wedge plates is parallel to the surface of the CFRP lamella. The interaction between the lamella and the wedge plates produces friction force. Furthermore, the continuous teeth on the clamping surface of the wedge plates increases the roughness and friction force between the plates and the CFRP lamella. The front and end of the wedge plates were chamfered to avoid locally crushing the CFRP lamella during tensioning. The anchor has a cylinder exterior and a wedge-shaped cavity interior, which can reduce the damage caused by the stress concentration effect in the anchorage.

2.2.2. Finite element analysis

Both finite element analysis and experimental study were carried out to verify the reliability and validity of the wedge-shaped clamp anchorage. A three-dimensional finite element model was developed by following the dimensions of the wedge-shaped clamp anchorage, as shown in Fig. 2. The model of the wedge-shaped clamp anchorage was established in the general finite element analysis (FEA) software ABAQUS [23]. The geometry model is shown in Fig. 3, where X-axis is the longitudinal direction (parallel to the fiber direction of the CFRP lamella) and Y-axis and Z-axis are the transverse directions (perpendicular to the fiber direction). Since the anchorage system was symmetric along both X-Y and X-Z planes, only one-quarter model was analyzed to improve the computing speed.

Both the wedge plates and the barrel were made with a typical isotropic material 42CrMo alloy steel. The mechanical properties are shown in Table 2. However, the CFRP is a typical linear orthotropic material and its material properties in the fiber direction are considerably different from those perpendicular to the fiber direction. Table 3 lists the engineering constants and material strengths of the CFRP used in the model in various directions. Among them, E represents the elastic modulus, G represents the shear modulus, ν represents the Poisson's ratio, S represents the strength, subscript 1 represents fiber direction, 2 and 3 represent perpendicular to the fiber direction, upper t represents tension, c represents compression. The CFRP lamellas used were provided by Shanghai Hummer Construction Technology Co., Ltd. [24]. The width of the lamella was 20 mm and the thickness was 3 mm, so the cross-sectional area

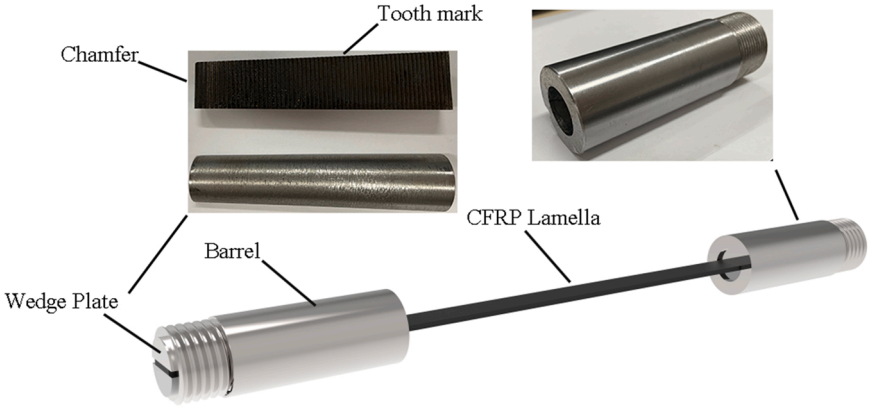

Fig. 1. Schematic diagram of wedge-shaped clamp anchorage.

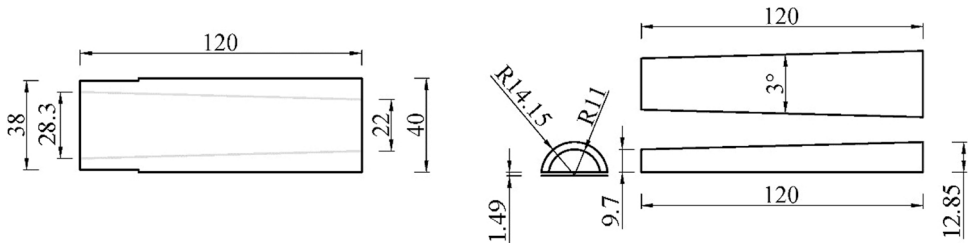

Fig. 2. Dimensional diagram of wedge-shaped clamp anchorage (Unit: mm)., (a) Barrel (b) Wedge plate.

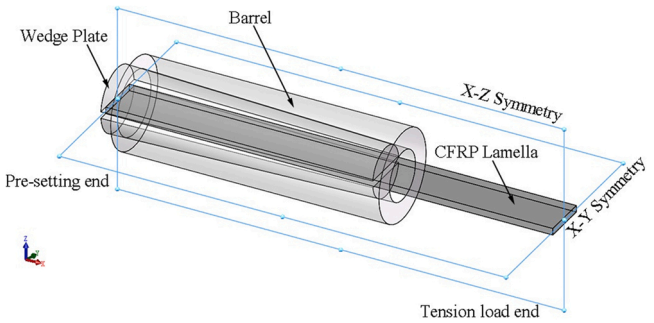

Fig. 3. Three-dimensional view of wedge-shaped clamp anchorage.

Table 2
Mechanical properties of anchor metal material.

Material	Tensile strength	Yield strength	Elastic modulus	Elongation at break	Impact toughness	Hardness
42CrMo alloy steel	1080 MPa	930 MPa	210 GPa	12%	78 J/cm^2	$\leq$ 217HB

Table 3
Engineering constant and material strength of CFRP lamella in all directions.

Material constant	Value	Strength parameter	Value
E_1	165 GPa	$S_{t\ 11}$	2400 MPa
E_2=E_3	12 GPa	$S_{c\ 11}$	-1500 MPa
G_{12}=G_{13}	9 GPa	$S^t_{22} = S_{t\ 33}$	80 MPa
G_{23}	6 GPa	$S_{c22} = S_{c\ 33}$	-200 MPa
υ_{12}=υ_{13}	0.3	S_{12} =S_{13}	150 MPa
υ_{23}	0.33	S_{23}	140 MPa

was 60 mm^2. All parameters in Table 2 and Table 3 were measured through material testing by the producer following relevant standards [25–27]. As can be seen from Table 3, the elastic modulus and the strength in the fiber direction are significantly greater than those in two directions perpendicular to the fiber direction. Moreover, the tensile strength in the fiber direction is greater than the compressive strength in the same direction, while the tensile strength perpendicular to the fiber direction is smaller than the compressive strength in the same direction.

The incompatible mode eight-node brick element (C3D8I) in ABAQUS was used to model the CFRP lamella and wedge-shaped

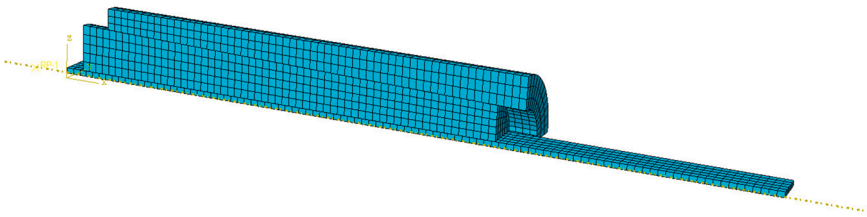

Fig. 4. Meshing situation of a one-quarter anchorage system.

clamp anchorage. The C3D8I element is an improved version of the C3D8 element, in which the shear locking is removed and volumetric locking is significantly reduced. It has high accuracy and is able to avoid the potential non-convergence problems in some complex stress conditions like the CFRP clamp anchor. Many other researchers also adopted the C3D8I element to model CFRP lamellas and achieved satisfying results [28–30]. The structured mesh generation technology of ABAQUS was adopted, combined with hexahedral element shape options, to model CFRP lamella, round barrel and two half-round wedge plates. In order to achieve high accuracy and acceptable computing time, the whole model adopted a 2 mm × 2 mm mesh size and 4400 elements were finally generated. The similar mesh size was used in the previous literature [31] as well. The completed FE model is shown in Fig. 4. Furthermore, the friction coefficient between the CFRP lamella and the wedge plates was set to 0.3 according to the friction test result. The rear end of the barrel was dynamically coupled with a fully consolidated fixed boundary, and two symmetry planes (XY and XZ planes) were applied symmetric constraints in corresponding directions, respectively. Two loading steps were set for the anchorage system, and the nonlinear numerical calculation was conducted. Step 1 was the pre-setting loading, which made the wedges plates contact tightly with the barrel [31]. In step 2, a tensile load was applied at the loading end of the CFRP lamella, which increased from 0 until the failure of the CFRP lamella. The boundary and load conditions are shown in Fig. 5.

The von Mises stress criterion was adopted as the fourth strength criterion to predict the failure of the metal material, which was suitable for ductile materials. Since the CFRP lamella is an orthotropic material, the von Mises stress cannot be used as an output parameter for the CFRP lamella. In order to predict the failure of CFRP lamella, the three-dimensional Hashin failure criterion was adopted to predict the failure of CFRP lamella and the UMAT subroutine was programmed, which could distinguish fiber failure modes and matrix failure modes, as well as tensile failure conditions and compression failure conditions [32].

2.2.3. Finite element analysis results

The von Mises stresses of the barrel and two wedge plates are shown in Figs. 6 and 7 respectively. Although a one-quarter model was established during the analysis state, mirroring techniques were used in post-processing to facilitate the presentation of the results, and the entire model of each component is presented. It is evident that there was no failure at the barrel and two-wedge clamps during the tensioning CFRP lamella as the maximum von Mises stresses for both barrel and two-wedge clamps were smaller than the yield strength (930 MPa) of 42CrMo alloy steel.

Fig. 8 shows the longitudinal stress (S11) distribution along with length and width directions. As can be seen, the contact pressure on the CFRP lamella was distributed over the whole length and width of the CFRP lamella. Moreover, there was no significant stress concentration at the CFRP lamella near the anchorage exit (i.e. the intersection of the anchorage and free sections) indicating that the CFRP lamella would not fail due to stress concentration. The average ultimate longitudinal stress (S11) of the free section reached 2239 MPa, reaching 93.3% of the theoretical material strength.

Fig. 9 shows the distribution of four Hashin failure indices of CFRP lamella. It can be seen that only the fiber tensile failure index reaches 1, which indicates that the failure mode of CFRP lamella is fiber tensile failure.

Fig. 10 shows the S11 stress distribution graphs under varied overall displacement. It can be seen that with the increase of displacement, the stress of the overall CFRP lamella gradually rose. Moreover, the stress of the free section rose almost evenly, whereas the stress change of the anchorage section was very uneven. The stress of the part near the anchorage front increased relatively quickly, while that of the part near the anchorage rear basically did not increase, even reduced to negative values.

2.2.4. Experimental verification

The tensile test of CFRP lamella stay-cables with the above wedge-shaped clamp anchorage was carried out to validate the FEA results. There were three specimens prepared and tested. The focuses of the test included the anchorage bearing capacity, the anchorage efficiency and the failure mode of the specimens.

The wedge-shaped clamp anchorages used in this experiment were made of 42CrMo alloy steel through the wire cutting process. The whole barrel was cut and drilled. The external taper of the wedge plates was equal to the internal taper of the barrel, and there were continuous teeth on the CFRP lamella contact surface. The dimensions of the two wedge plates were exactly identical. CFRP lamellas were provided by Shanghai Hummer Construction Technology Co., Ltd. [24], and the parameters used in the test are the same as those in Tables 2 and 3.

During the fabrication of the specimens, first the surface of the barrel and wedge plates were cleaned with acetone reagent, especially to remove dust and oil residue from the cutting process on the tooth pattern of the wedge plates. Then the two wedge plates

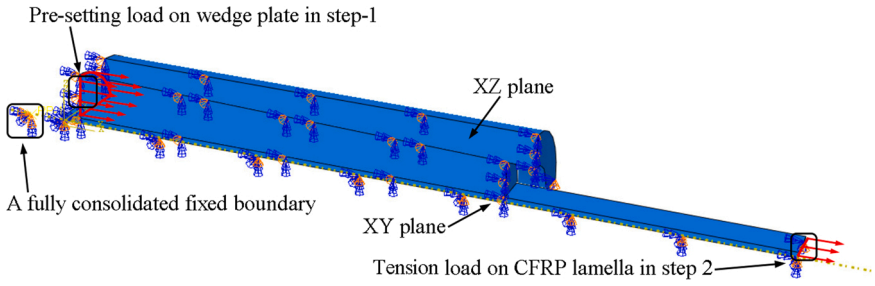

Fig. 5. Boundary and load conditions of one-quarter anchorage system.

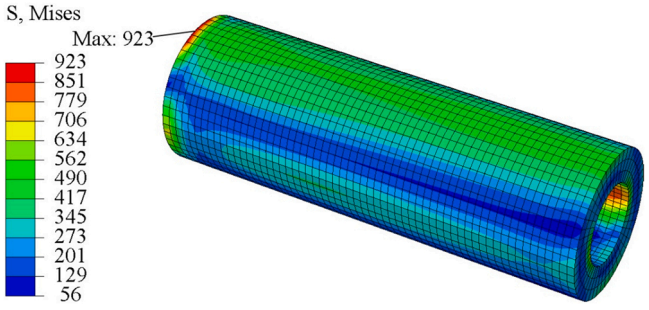

Fig. 6. Von Mises stress nephogram of the barrel (Unit: MPa).

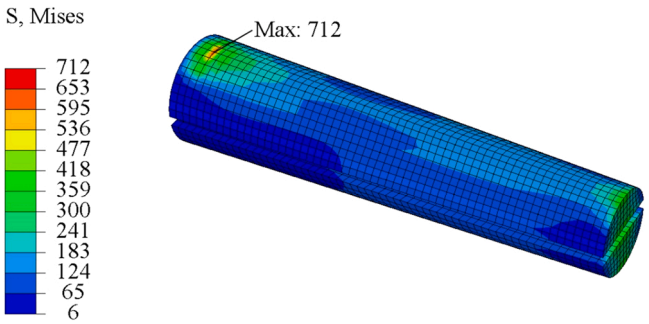

Fig. 7. Von Mises stress nephogram of the two wedge plates (Unit: MPa).

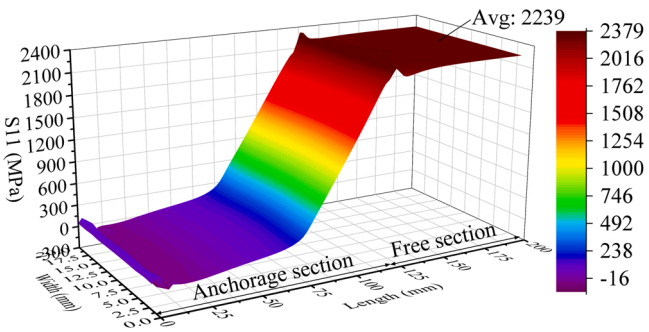

Fig. 8. The longitudinal stress (S11) distribution in the length and width directions of the CFRP lamella.

were placed for holding the CFRP lamella on top of each other, with the CFRP lamella centered and the large end face of the two plates and the end face of the CFRP lamella fixed in the same vertical plane, so that the outer contour of the three formed an approximate circle. Then the convex surfaces of the upper and lower wedge plates were evenly lubricated to make it easier for the wedges to embed in the barrel. Furthermore, the barrel was slowly snapped in from the small end of the wedge plates in the direction from the large end to the small end until the wedge plates and the barrel were just in contact, with the large end of the two plates and the end of the CFRP lamella fixed in the same vertical plane during this process. Then the micro-pretensed anchor was placed into the tooling part and applied a preload of 100 kN with a hydraulic jack. Finally, the other end of the specimen was installed according to the same procedure abovementioned and screw on the anchoring head at each end to complete the whole specimen. The flow chart of the fabrication process of tensile test specimens is shown in Fig. 11.

The tensile test was conducted using an MTS testing machine with 300 kN tensile capacity. The specimens were loaded with displacement control monotonic tension at a rate of 2 mm/min until failure occurred. During the installation of specimens, the anchorage was connected to the square conversion head clamped to the test machine by means of threaded rods at the top and bottom ends, as shown in Fig. 12(a). Before starting each test, the specimen was first connected to the upper and lower square conversion heads via the threaded rod, then the upper and lower beams of the test machine were adjusted to the appropriate distance and finally, the two square conversion heads were slowly and synchronously embedded into the upper and lower clamping heads of the test machine to keep the specimen straight throughout the embedding process. The quantities measured during the test included the test load and the longitudinal strain of the CFRP lamella. The strain was measured by an extensometer, arranged in the free section of the specimen. It

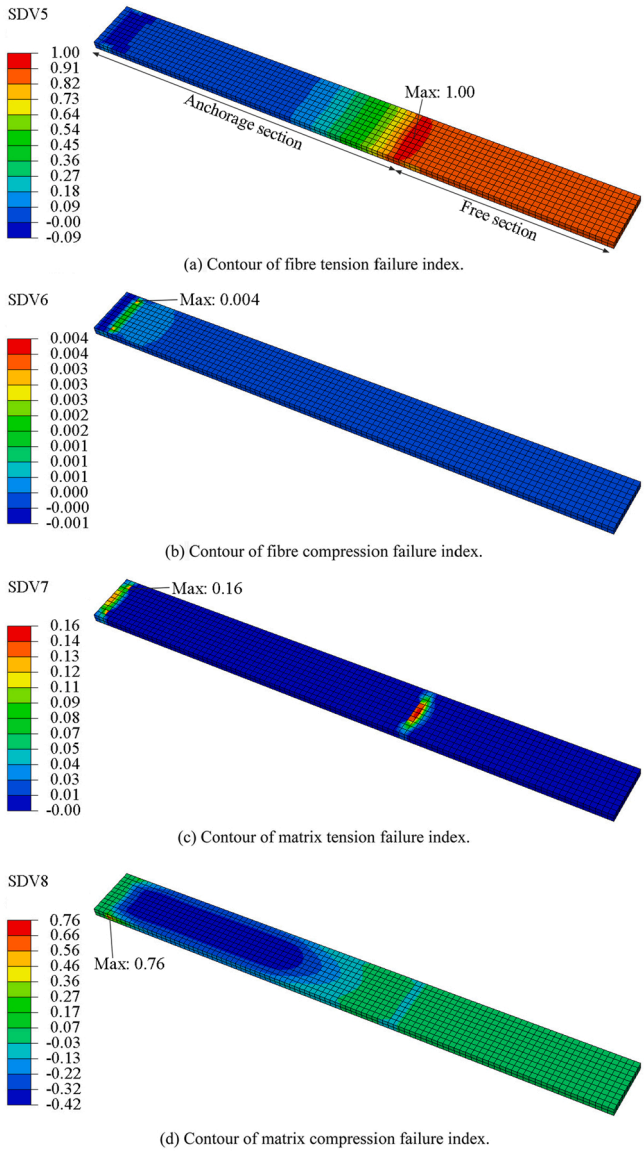

Fig. 9. Contours of CFRP lamella failure indices., (a) Contour of fibre tension failure index., (b) Contour of fibre compression failure index., (c) Contour of matrix tension failure index., (d) Contour of matrix compression failure index.

measured the tensile strain in the axial direction of the specimen. The experimental setup is shown in Fig. 12.

The three specimens after testing are shown in Fig. 13. It shows that the failure of the specimens were mainly the fiber explosion in the free section of the CFRP lamella. It should be noted that there was also a little splitting of CFRP during the test, especially for specimen 1. The test results showed the specimen 1 had the smallest ultimate tensile force, too. After the test, it was found the CFRP lamellas in the anchorage section were still in good condition without obvious damage. This phenomenon was the same as obtained in FEA.

The test results are listed in Table 4. The actual ultimate tensile force was taken as the maximum value set in the MTS test machine and the specimen failed during tension. According to the ultimate tensile strength (2400 MPa) and the cross-sectional area of the CFRP lamella (60 mm^2), the theoretical ultimate tensile force can reach 144 kN through calculation. The anchorage efficiency was defined as the ratio of the actual ultimate tensile force of each specimen to the theoretical ultimate tensile force. The load-displacement curves of the three specimens are shown in Fig. 14. As can be seen, the highest point of the load-displacement curves of the three specimens reaches 129.4 kN, and the average anchorage efficiency of the test is 87.2%. Furthermore, the comparison of the stress-strain curves of the three specimens and the aforementioned FEA results is shown in Fig. 15. As can be seen, the stress-strain curve from the FEA is very similar to those from the experiment, proving the correctness of the FEA result, and all the curves are inclined straight lines before failure, verifying that the CFRP lamella is a typical linear elastic material.

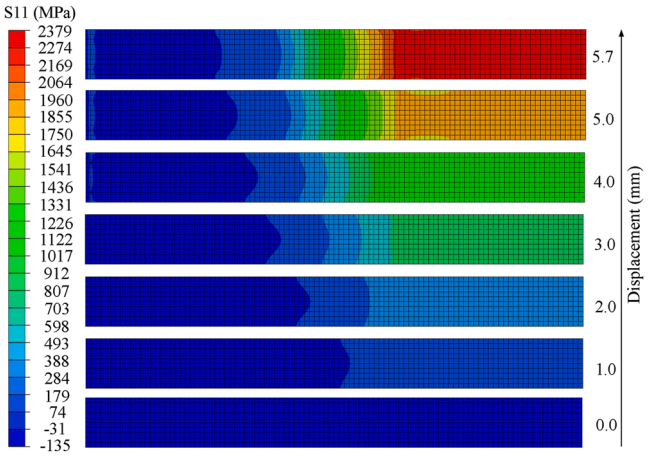

Fig. 10. The longitudinal stress (S11) distribution graphs under varied overall displacement.

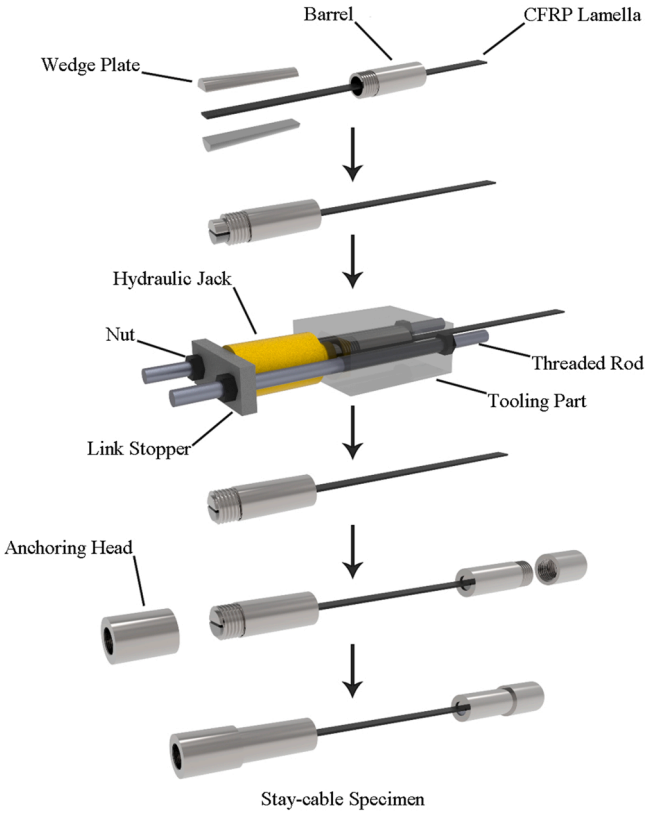

Fig. 11. Fabrication process of the specimen.

In summary, the FEA and experiment showed that the CFRP lamella anchored with the wedge-shaped clamp anchorage was able to achieve 94.3% and 87.2% of its theoretical ultimate load capacity, respectively. The difference between the numerical and experimental results was only 7.1%, which shows they were in good agreement. The final failure was mainly the fiber explosion failure in the free section of the CFRP lamella, while the anchorage section and the anchor itself were not damaged during the loading process. It is therefore shown that the wedge-shaped clamp anchorage proposed in this study is a reliable design to anchor CFRP lamella. It should be noted that the wedge-shaped clamp anchorage still needs further optimization to make its anchorage efficiency greater than or equal to 95%, which is specified in the standard [33] for practical use.

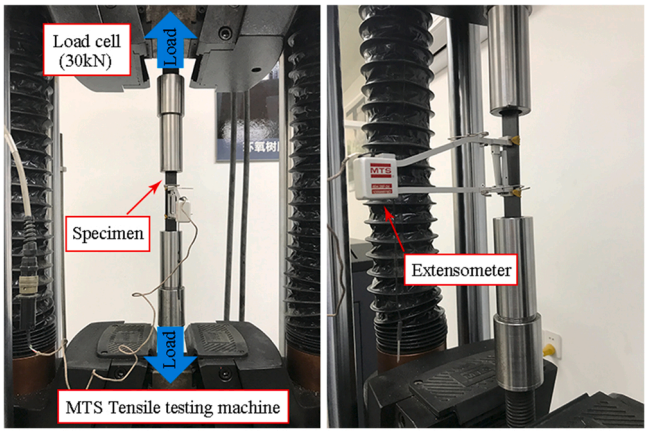

(a) Installation of specimens (b) Layout scheme of extensometer

Fig. 12. Tensile test setup., (a) Installation of specimens (b) Layout scheme of the extensometer.

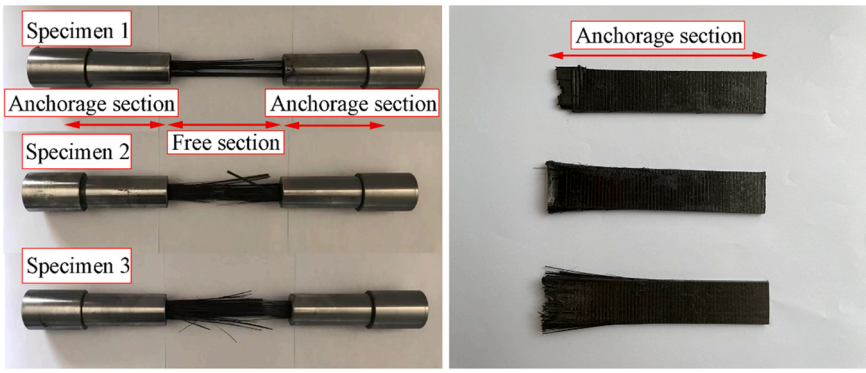

Fig. 13. Failure mode of three specimens.

Table 4
Comparison of numerical and experimental ultimate tensile loads.

Specimen ID	Actual ultimate tensile force (kN)	Actual ultimate tensile stress (MPa)	Theoretical ultimate tensile force (kN)	Anchoring efficiency (%)
Specimen 1	121.7	2028	144.0	84.5
Specimen 2	125.6	2093	144.0	87.2
Specimen 3	129.4	2157	144.0	89.9
FEA	134.3	2238	144.0	93.3

3. Force measurement of CFRP lamella stay-cable based on microwave

3.1. Theoretical basis

3.1.1. Microwave pickup technology

The process of microwave radar picking up the cable vibration is based on radar remote sensing technology and differential interferometry technology. The equipment used is mainly composed of a tripod, a computer control unit, an energy supply unit and a radar control unit. The radar control unit is installed on a tripod equipped with a 3D rotating head to ensure that the radar monitoring direction is adjusted. At the same time, the radar unit is equipped with two antennas for transmitting and receiving microwave signals respectively [34]. First, the radar continuously transmits a linear frequency modulated continuous wave (FMCW) signal to the stay-cable, then goes to frequency modulation to realize the echo reception. Then it uses the differential interferometry technology to calculate and analyze the phase difference of the microwave reflected by the stay-cable at different times. Finally, it obtains the high-frequency micro-deformation information on the surface of the stayed cable in a continuous period of time, which is the time-domain signal of the stayed cable vibration [34]. The principle is shown in Fig. 16.

In Fig. 16, d is the displacement of the measuring point of the cable between two measurements in the microwave direction, which

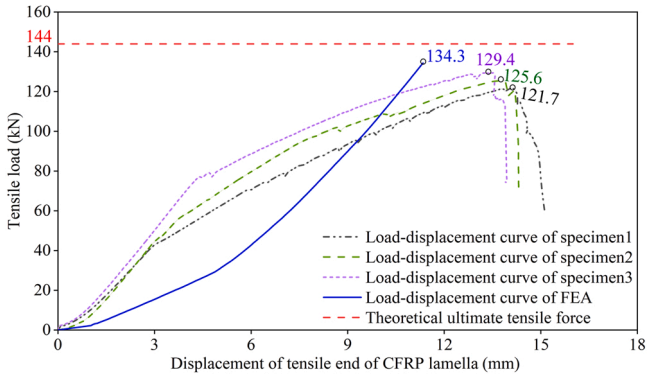

Fig. 14. Load-Displacement curves of three specimens and finite element analysis.

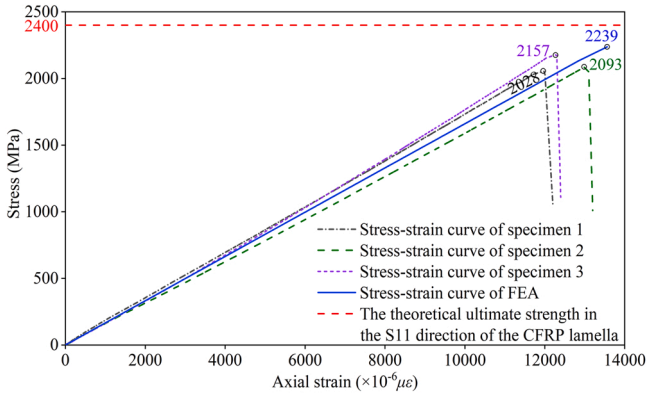

Fig. 15. Stress-strain curves of three specimens and finite element analysis.

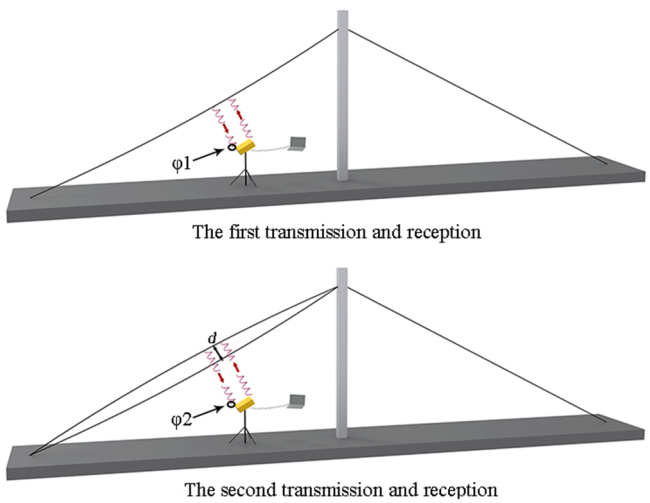

Fig. 16. Schematic diagram of microwave radar picking cable vibration.

can be calculated by Eq. (1):

$$d = \frac{\lambda}{4\pi}(\varphi_2 - \varphi_1) \tag{1}$$

In the above equation, λ is the working wavelength of the radar, φ_1 is the phase of the first target measurement, φ_2 is the phase of the second target measurement. The microwaves emitted by the microwave radar are distributed in a fan shape and within a certain

distance range. It is possible to measure the forces of multiple cables at the same time, and the forces at different positions of each cable can also be measured [35]. The microwave can pass through the polyethylene (PE) sheath and reach the high-strength steel wire in the stay-cable. This can ensure the authenticity and reliability of the measurement results and is especially suitable for parallel strand stay-cables.

3.1.2. Time-frequency domain transformation

After the microwave radar obtains the vibration time-domain signal $d(t_s)$ by accurately measuring the cable displacement, it needs to undergo a discrete Fourier transform to obtain the frequency domain signal $X(f_d)$ of the cable vibration displacement. That is, the vibration frequency of the stay-cable is obtained by Fourier transform on the time history curve of the vibration displacement of the stay-cable. The $X(f_d)$ can be calculated using Eq. (2).

$$X(f_d) = \int_0^{T_x} d(t_s)\exp(-j2\pi f_d t_s)dt_s \tag{2}$$

In the equation: T_x is the deformation observation time; f_d is the frequency resolution, and the two are inversely proportional [36].

3.1.3. Calculation of cable force

Each cable of a cable-stayed bridge is usually more than 10 m long. One end of the cable is connected to the bridge tower, and the other end is connected to the bridge deck. Although each cable is made of multiple steel wires or steel strands, relative to the length of the entire cable and the tension it bears, it can be approximated as an ideal stringing form with hinged ends and negligible weight.

(a) Site photos of the test bridge.

(The red circles in the picture indicate the CFRP cables to be measured.)

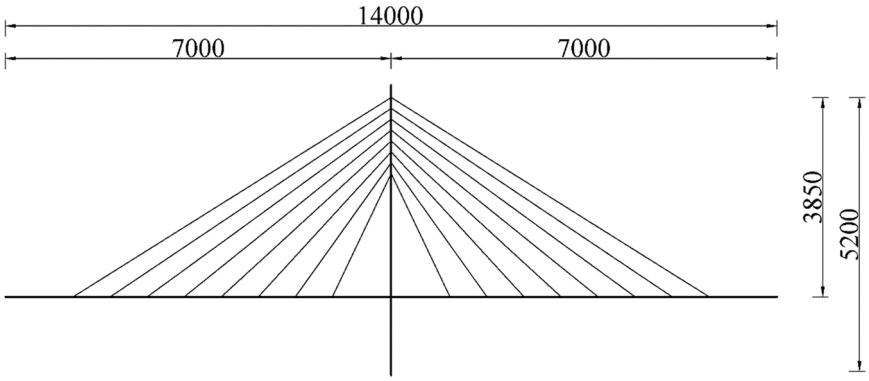

(b) Front view of the test bridge (Unit: mm).

Fig. 17. The cable-stayed model bridge used in the model test., (a) Site photos of the test bridge. (The red circles in the picture indicate the CFRP cables to be measured.) (b) Front view of the test bridge (Unit: mm).

According to the flexible string vibration theory [37], the corresponding undamped free vibration equation can be obtained by Eq. (3):

$$\rho \frac{\partial^2 u}{\partial^2 t} - T \frac{\partial^2 u}{\partial^2 x} = 0 \tag{3}$$

In the above equation, $u(x,t)$ is the lateral displacement of each point on the cable at any time t; ρ is the linear density of the cable; T is the internal tension of the cable.

The relationship between cable force and frequency can be obtained by Eq. (4):

$$T = 4\rho l^2 \left(\frac{f_n^2}{n^2}\right) = 4\rho l^2 \left(\frac{f_n}{n}\right)^2 = 4\rho l^2 f_1^2 \tag{4}$$

where, l is the calculated length of the stay-cable; f_n is the natural frequency of the n^{th} order; n is the order of the natural frequency; f_1 is the fundamental frequency, which is usually taken from the first peak in the spectrogram or obtained by using the frequency difference between two adjacent peaks.

3.2. Model test

3.2.1. Installation of CFRP lamella stay-cable

The bridge used in this experiment is a single tower self-anchored cable-stayed model bridge (as shown in Fig. 17), and all stay-cables are arranged in a fan-shaped arrangement of double cable planes. The whole bridge has 8 pairs of cables (16 in total). The horizontal spacing of cables at the beam is 715 mm, and the vertical spacing at the tower is 210 mm. There were two CFRP lamella stay-cables installed in the bridge, as shown in Fig. 17(a). The length of the two CFRP cables is 7700 mm.

A complete CFRP lamella stay-cable consists of a CFRP lamella, a pair of wedge-shaped clamp anchorages and a cable regulator. The CFRP lamella stay-cable was installed according to the specimen production process described in Section 2.2.4. After the CFRP stay-cable had been installed, the anchor heads were fitted to both ends. The tower and deck of the cable-stayed model bridge had been fitted with high-strength eyebolts. One end of the cable was connected to the eyebolt of the bridge tower by employing a U-shaped connection with a threaded rod, the other end was connected to the cable regulator and then to the eyebolt of the bridge deck by means of an ear plate. Furthermore, the pressure sensor was also installed on the threaded rod of the cable regulator. The connection details of the CFRP cable and bridge deck are shown in Fig. 18. The installing and measuring process of the two CFRP cables was the same.

The outer sleeve of the cable regulator was connected at both ends with two threaded rods set in opposite directions, one end was connected to the anchor head at the lower end of the cable and the other end was connected to the ear plate on the bridge deck. By turning the outer sleeve clockwise, both threaded rods were screwed into the barrel at the same time and the cable was gradually tensioned.

3.2.2. Cable force measurement using microwave radar

Before the test begins, the radar was fixed in a suitable position on the bridge deck and positioned so that the plane formed by the transmitting beam of radar was as perpendicular as possible to the stay-cable measured. On initial observation of the reflected waveforms measured by radar, the radar echoes reflected by the stay-cable would be significantly different from those reflected by the environment. The radar itself had a distance measurement function, which could be used to determine the distance of each radar waveform peak in turn corresponding to each stay-cable, and could also be used to further confirm the distance between stay-cable and radar by using an auxiliary optical rangefinder to measure the distance between the stay-cable and the radar. The radar would automatically record the sight distance, vibration amplitude and other test data of all the cables according to time, transform the measured cable time domain signal to frequency domain for data analysis, and obtain the fundamental frequency and vibration frequency of each order of the cable to find the cable force. In the test, the traditional pressure sensor method and strain gauge method were also used for comparison. The pressure sensor was mounted on the threaded rod of the cable regulator and the strain gauges were attached to the middle of the CFRP lamella in three equally spaced locations along its length. The arrangement of the cable force measurement is shown in Fig. 19.

In the test, there were a total of seven working conditions, and the CFRP cables were tensioned step by step. In the process of tensioning, the outer sleeve of the cable regulator was rotated clockwise by the wrench. After each tension condition was completed, the measurement results of microwave radar, pressure sensor and strain collector were recorded.

The length of the stay-cable measured in the test was relatively short and could be divided into two parts: CFRP and steel components. The density of CFRP was small and the density of steel components was relatively large, which led to inaccurate cable linear density calculated by conventional methods. Therefore, the "equivalent linear density" was used. In the first working condition of the test, the fundamental frequency (f_1) measured by microwave radar, the cable force T_1 measured by the pressure sensor and the calculated length L of the cable were taken into Eq. (5),

$$\rho_e = \frac{T}{4l^2 f_1^2} \tag{5}$$

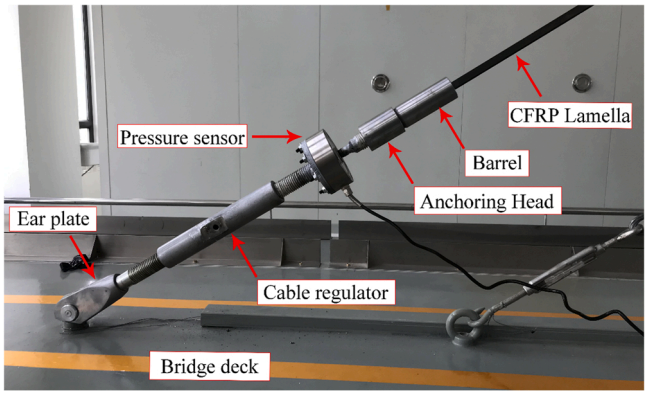

Fig. 18. Connection details of cable and bridge deck.

The calculated linear density ρ_e was the equivalent linear density of the stay-cable.

3.2.3. *Determination and validity of the cable force measurement results*

Fig. 20 shows the spectrogram curve of working condition 1 obtained by the microwave radar. As can be seen, the fundamental frequency (f_1) of the CFRP cable was 7.776 Hz. Furthermore, the cable force measured by the pressure sensor (T_1) was 4200 N, and the length of the cable (L) was 7.7 m. The three parameters were taken into the above Eq. 5. The equivalent linear density (ρ_e) of the CFRP lamella stay-cable was 0.293 kg/m by calculation. However, the linear density of the CFRP lamella was only 0.114 kg/m, which is significantly smaller than the equivalent one. If the linear density of the CFRP lamella was used to calculate the CFRP cable force, the error would be considerably large.

The spectrograms of working conditions 2–7 measured by the microwave radar are shown in Fig. 21. The pressure sensor and strain collector were always measured in real-time during the seven working conditions. After each condition had been loaded and stabilized,

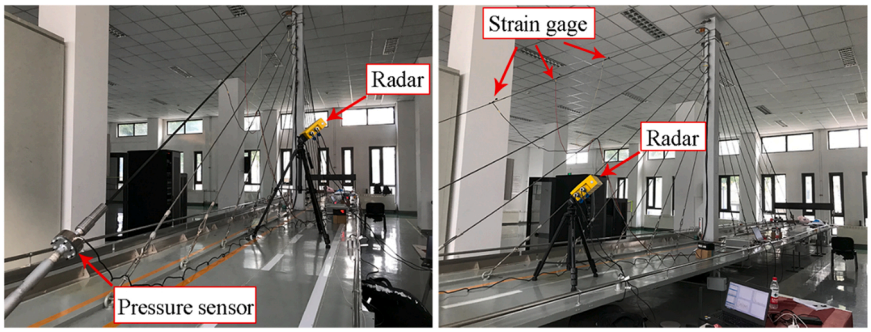

Fig. 19. Measuring arrangement of cable force.

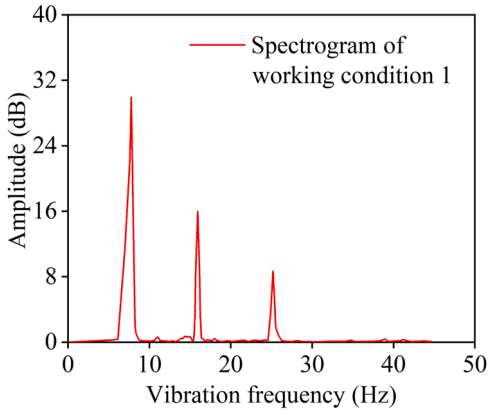

Fig. 20. Spectrograms of working condition 1 measured by radar.

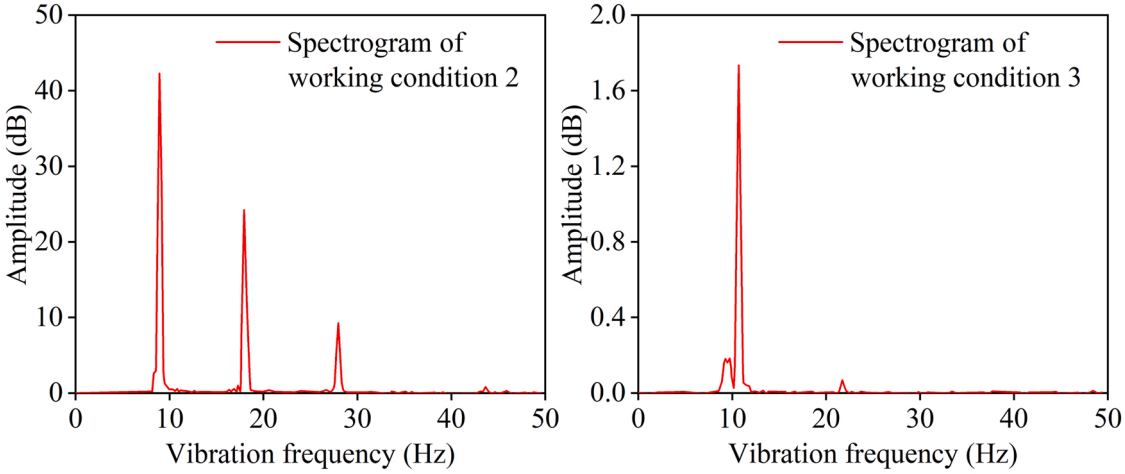

(a)Working condition 2

(b)Working condition 3

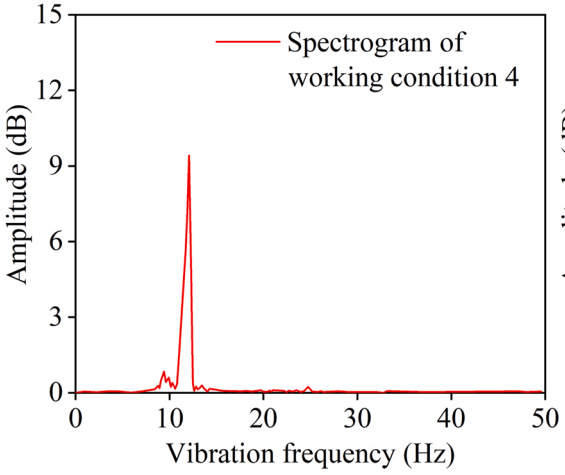

(c)Working condition 4

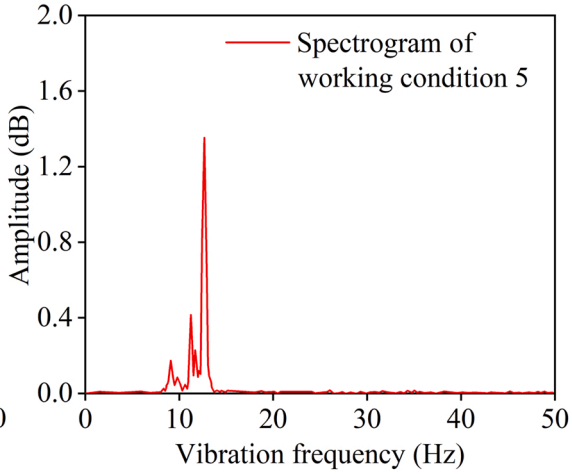

(d)Working condition 5

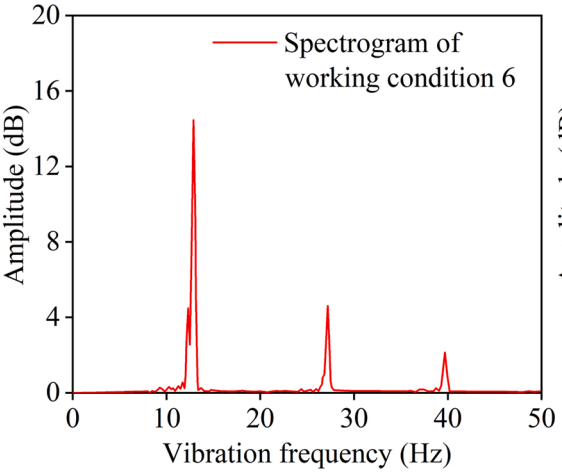

(e)Working condition 6

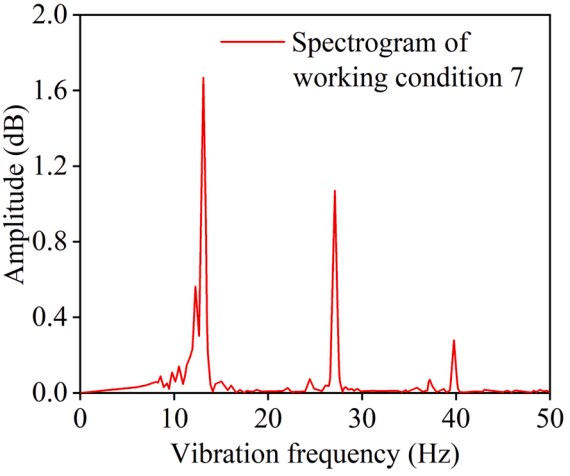

(f)Working condition 7

(caption on next page)

Fig. 21. Spectrograms of working conditions 2–7 measured by radar., (a)Working condition 2 (b)Working condition 3, (c)Working condition 4 (d) Working condition 5, (e)Working condition 6 (f)Working condition 7.

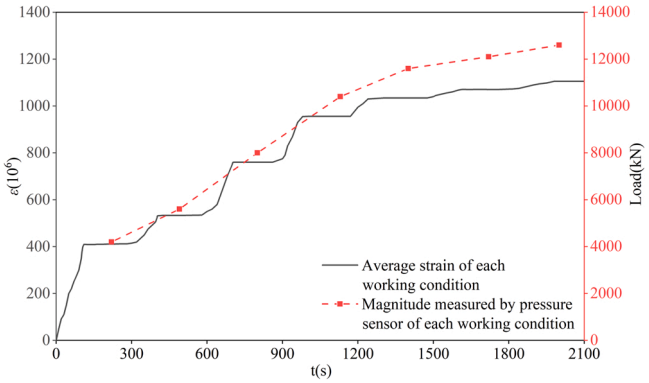

Fig. 22. Collection results of the pressure sensor and strain gauge.

Table 5
Comparison of measurement results of pressure sensor, strain gauge and radar.

Working condition	Calculating length (m)	Linear density of the cable (kg/m)	Fundamental frequency measured by radar (Hz)	Cable force measured by radar (CF_{radar}) (N)	Cable force measured by pressure sensor ($CF_{pressure\ sensor}$) (N)	Cable force measured by strain gauge ($CF_{strain\ gauge}$) (N)	$\frac{CF_{radar}}{CF_{pressure\ sensor}}$	$\frac{CF_{radar}}{CF_{strain\ gauge}}$
1	7.7	0.293	7.776	4200	4200	4056	1.00	1.04
2	7.7	0.293	8.942	5556	5600	5265	0.99	1.06
3	7.7	0.293	10.693	7945	8100	7512	0.98	1.06
4	7.7	0.293	12.075	10132	10400	9465	0.97	1.07
5	7.7	0.293	12.661	11139	11600	10235	0.96	1.09
6	7.7	0.293	12.887	11540	12100	10564	0.95	1.09
7	7.7	0.293	13.113	11948	12600	10897	0.95	1.10
						Mean	0.97	1.07
						COV	1.87%	1.96%

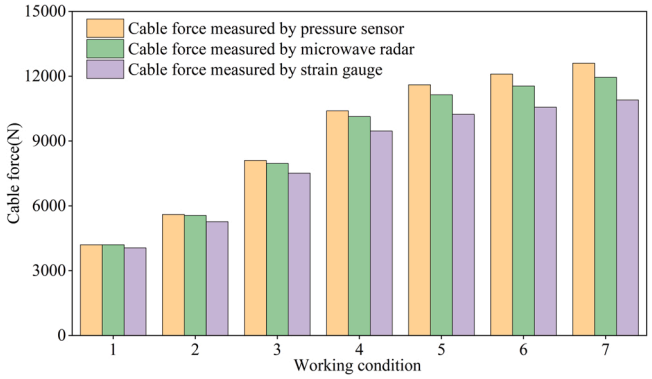

Fig. 23. Comparison of the measurement results of the pressure sensor, strain gauge and radar.

the pressure sensor's magnitude was read in real-time through the matching display instrument, and the dynamic collector recorded the change of strain on the CFRP lamella cable in real-time, the results of both are shown in Fig. 22.

The comparative analysis of the measurement results of the three methods, i.e. pressure sensor, strain gauge and microwave radar with the increase of the cable force under different working conditions are shown in Table 5 and Fig. 23.

From the above results, it can be concluded that the cable force measured by microwave radar is in general agreement with that measured by the pressure sensor and strain gauges, where the mean ratio and coefficient of variation (COV) were 0.97 and 1.87% respectively when compared with pressure sensor method and 1.07 and 1.96% respectively when compared with strain gauge method,

indicating that the cable force results measured by microwave radar were reliable. Although both the pressure sensor and strain gauge are mature methods for cable force measurement, the pressure sensor method is usually regarded as the accurate one [18]. In this model test, the error of the strain gauge method was probably caused by the temperature related effects; the error of the microwave radar method was not related to the radar itself, but because the CFRP cable measured is relatively short and its mass distribution is uneven, which is not an ideal string with negligible weight. However, this systematic error of the microwave radar method was proved to be small by this model test, and it will be even smaller for the real CFRP stay cables with a longer length and evener mass distribution. Furthermore, the non-contact microwave cable force measurement method took less than 2 min to measure the cable force for each cable, while the pressure sensor method and strain gauge method took more than 30 min to measure the cable force for each cable, indicating that the measurement speed was increased more than 15 times, which can significantly improve the efficiency of the construction phase. The main purpose of the present measurement test was to verify the effectiveness and accuracy of the microwave radar measuring the CFRP lamella stay-cable. Although there was only one CFRP lamella, it had already proved that the microwave did not penetrate or be absorbed but reflected by the CFRP lamella and was received by the radar. Consequently, this technology can be also used for the CFRP parallel lamella stay-cable, which has some of the same parallel CFRP lamellas, and they are not only tied into a whole by the sheath and filling material but also have an equal vibration frequency.

4. Conclusion

The measurement of cable force has long been an important part of bridge construction and health monitoring, especially for stay-cables. We introduced a non-contact microwave technology based on vibration frequency pickup to measure the force of the CFRP lamella stay-cable. First, the advantage of CFRP lamella in terms of anchoring compared with CFRP rod was demonstrated. Then, a wedge-shaped clamp anchorage suitable for CFRP lamella was proposed and investigated by FE and experimental analyses. Finally, a model test was conducted and the force of CFRP lamella stay-cable was measured by the microwave radar, which was also compared with the traditional cable force measurement methods. The following conclusions were drawn:

(1) The CFRP lamella is more efficient to anchor than the CFRP rod. When the CFRP lamella and rod have equal cross-sectional area and anchorage length, the anchorage area of the CFRP lamella is approximately twice that of the CFRP rod. Moreover, the anchorage area of CFRP lamella is almost proportionally increasing with the increase of the width of CFRP lamella.
(2) The wedge-shaped clamp anchorage proposed in this study is a reliable design for anchoring CFRP lamella. The finite element analysis and experiment showed that the CFRP lamella anchored with the wedge-shaped clamp anchorage was able to achieve 93.0% and 87.2% of its theoretical ultimate load capacity, respectively. The difference between the numerical and experimental results was only 5.8%. The final failure was mainly the fiber explosion failure in the free section of the CFRP lamella, while the anchorage section and the anchor itself were not damaged during the loading process.
(3) The accuracy of non-contact microwave cable force measurement is able to meet the engineering requirements, and the measurement time is greatly shortened. The mean ratio and coefficient of variation (COV) were 0.97% and 1.87% respectively when compared with the pressure sensor method and 1.07% and 1.96% respectively when compared with the strain gauge method. Thus, it can be used to measure the force of CFRP cables. Furthermore, for a relatively short CFRP cable in which the anchorage occupies a relatively large length, the equivalent linear density rather than the material linear density of CFRP should be used in the calculation of the cable force.

Declaration of Competing Interest

The authors declare that they have no known competing financial interests or personal relationships that could have appeared to influence the work reported in this paper.

Acknowledgement

The authors gratefully acknowledge the financial support provided by the National Natural Science Foundation of China (NSFC 51908012), the Postdoctoral Research Foundation of China (2019M660962) and the International Research Cooperation Seed Fund of Beijing University of Technology (2021B11).

References

[1] Y. Liu, B. Zwingmann, M. Schlaich, Carbon fiber reinforced polymer for cable structures - a review, Polymers 7 (10) (2015) 2078–2099.
[2] U. Meier, Proposal for a carbon fibre reinforced composite bridge across the Strait of Gibraltar at its narrowest site, Proc. Inst. Mech. Eng., Part B: Manag. Eng. Manuf. 201 (2) (1987) 73–78.
[3] V.M. Karbhari, Use of composite materials in civil infrastructure in Japan (WTEC report), International Technology Research Institute, World Technology (WTEC) Division,, 1998.
[4] H. Meier, U. Meier, R. Brönnimann, Zwei CFK-Kabel für die Storchenbrücke, Schweiz. Ing. UND Archit.-SCHWEIZERISCHE Bauztg. 114 (44) (1996) 8–13.
[5] T. Tafsirojjaman, S. Fawzia, D. Thambiratnam, X.L. Zhao, Numerical investigation of CFRP strengthened RHS members under cyclic loading (Elsevier), Structures 24 (2020) 610–626.
[6] T. Tafsirojjaman, S. Fawzia, D.P. Thambiratnam, X.L. Zhao, Study on the cyclic bending behaviour of CFRP strengthened full-scale CHS members (Elsevier), Structures 28 (2020) 741–756.
[7] Y. Liu, Carbon Fibre Reinforced Polymer (CFRP) Cables for Orthogonally Loaded Cable Structures, Advantages and Feasibility, Logos Verlag Berlin, 2015.

[8] U. Meier, H. Meier, P. Kim, Anchorage device for high-performance fiber composite cables, U.S. Patent 5713169, (1998).
[9] Z. Fang, K. Zhang, B. Tu, Experimental investigation of a bond-type anchorage system for multiple FRP tendons, Eng. Struct. 57 (2013) 364–373.
[10] K. Zhang, Z. Fang, A. Nanni, J. Hu, G. Chen, Experimental study of a large-scale ground anchor system with FRP tendon and RPC grout medium, J. Compos. Constr. 19 (4) (2015), 04014073.
[11] X. Wang, J. Zhou, J. Song, W.U. Zhishen, Theoretical analysis on integral anchor for large-tonnage FRP composites cable, Acta Mater. Compos. Sin. 5 (2019) 1169–1178.
[12] B. Feng, X. Wang, Z. Wu, Static and fatigue behavior of multitendon CFRP cables with integrated anchorages, J. Compos. Constr. 23 (6) (2019), 04019051.
[13] R.L. Geffroy, The Laroin footbridge with carbon composite stay-cables, Proc. Footbridge (2002).
[14] H. Dehmous, H. Welemane, Multi-scale reliability analysis of composite structures–Application to the Laroin footbridge, Eng. Fail. Anal. 18 (3) (2011) 988–998.
[15] H. Andrä, M. Maier, Brückensanierung mit CFK-Lamellenspanngliedern, Faserverbundwerkstoffe-Innovationen im Bauwesen, Beiträge aus Praxis und Wissenschaft, 2005, pp. 65–76.
[16] F. Fischli, R. Clénin, A. De Silva, P. Chaemmangkang, Strengthening of structures with the CARBOSTRESS system, Asia-Pacific Conference on FRP in Structures (APFIS 2007), International Institute for FRP in Construction,, 2007, pp. 387–392.
[17] C. Li, R. Guo, G. Xian, H. Li, Innovative compound-type anchorage system for a large-diameter pultruded carbon/glass hybrid rod for bridge cable, Mater. Struct. 53 (4) (2020) 1–15.
[18] L. Zhang, G. Qiu, Z. Chen, Structural health monitoring methods of cables in cable-stayed bridge: a review, Measurement 168 (2021), 108343.
[19] G.K. Xiong, C.T. Zhou, Characteristics and applicability analysis of five methods for determination of cable force, Subgrade Eng. 2 (2012) 138–140.
[20] R. Geier, G. De Roeck, R. Flesch, Accurate cable force determination using ambient vibration measurements, Struct. Infrastruct. Eng. 2 (1) (2006) 43–52.
[21] T. Khuc, F.N. Catbas, Computer vision-based displacement and vibration monitoring without using physical target on structures, Struct. Infrastruct. Eng. 13 (4) (2017) 505–516.
[22] G. Zhang, Y. Wu, W. Zhao, J. Zhang, Radar-based multipoint displacement measurements of a 1200-m-long suspension bridge, ISPRS J. Photogramm. Remote Sens. 167 (2020) 71–84.
[23] A.U. Manual, Abaqus user manual, Abacus (2020).
[24] Hummer CFRP Lamella 2020 Technical report. Shanghai Hummer Construction Technology Co., Ltd. (2020).
[25] Standardization Administration of the People's Republic of China (SAPRC), "Test Methods for Properties of Resin Casting Body, GB/T 2567–2008 (In Chinese)," Beijing, China, (2008).
[26] Standardization Administration of the People's Republic of China (SAPRC), "Test method for tensile properties of oriented fiber reinforced polymer matrix composites, GB/T 3354–2014 (In Chinese)," Beijing, China, (2014).
[27] Standardization Administration of the People's Republic of China (SAPRC), "Metallic Materials-Tensile Testing at Ambient Temperature, GB/T 228–2002(In Chinese)," Beijing, China, (2002).
[28] W. Huang, R. Xu, J. Yang, Q. Huang, H. Hu, Data-driven multiscale simulation of FRP based on material twins, Compos. Struct. 256 (2021), 113013.
[29] X.T. Wang, B. Wang, Z.H. Wen, L. Ma, Fabrication and mechanical properties of CFRP composite three-dimensional double-arrow-head auxetic structures, Compos. Sci. Technol. 164 (2018) 92–102.
[30] R. Guedes, M. De Moura, F. Ferreira, Failure analysis of quasi-isotropic CFRP laminates under high strain rate compression loading, Compos. Struct. 84 (4) (2008) 362–368.
[31] F.M. Mohee, A. Al-Mayah, Development of an innovative prestressing CFRP plate anchor: numerical modelling and parametric study, Compos. Struct. 177 (2017) 1–12.
[32] Z. Hashin, Failure criteria for unidirectional fiber composites, J. Appl. Mech. 47 (1980) 329–334.
[33] Standardization Administration of the People's Republic of China (SAPRC), "Fiber reinforced polymer composites structural cables, GB/T 35156–2017 (In Chinese)," Beijing, China, (2017).
[34] I.H. Woodhouse, Introduction to microwave remote sensing, CRC press, 2017.
[35] C. Gentile, Deflection measurement on vibrating stay cables by non-contact microwave interferometer, NDT E Int. 43 (3) (2010) 231–240.
[36] C.W. Xiao, M.L. Zhu, S.Q. Zhu, Comparative study of cable tension measurement based on microwave radar method and vibration method, Munic. Eng. Technol. 38 (S01) (2020) 132–135.
[37] R. Narasimha, Non-linear vibration of an elastic string, J. Sound Vib. 8 (1) (1968) 134–146.